ACS APPLIED POLYMER MATERIALS

pubs.acs.org/acsapm Article

Confinement and Composition Effects on the Degradation Profile of Extruded PLA/PCL Nonwoven Fiber Blends

Kristian M. Van de Voorde, LaShanda T. J. Korley,* and Jonathan K. Pokorski*

Cite This: *ACS Appl. Polym. Mater.* 2021, 3, 3878−3890 Read Online

ACCESS | Metrics & More | Article Recommendations | Supporting Information

ABSTRACT: A vital characteristic of a nanofibrous scaffold for regenerative medicine is its ability to degrade *in vivo* at the same rate that a damaged tissue regenerates, while maintaining its mechanical properties for structural support. This work explores the degradation kinetics and mechanical properties of extruded nanofibers fabricated through blending two commonly utilized polyesters, poly(lactic acid) and poly(ε-caprolactone). Morphological effects are correlated to degradation rates of extruded nanofibers and reveal that morphology was coupled both to the blend composition and the multilayer coextrusion processing technique. Furthermore, the correlation of the resulting mechanical properties provides improved insights into the structure−property dynamics between hydrolysis and residual mechanical properties for semicrystalline polymers to better predict scaffold performance.

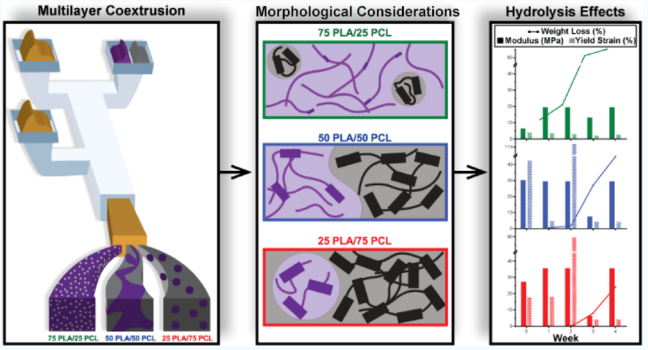

KEYWORDS: *poly(lactic acid), poly(ε-caprolactone), nanofibers, degradation kinetics, polyester blends*

Downloaded via CASE WESTERN RESERVE UNIV on August 10, 2022 at 19:01:44 (UTC).
See https://pubs.acs.org/sharingguidelines for options on how to legitimately share published articles.

INTRODUCTION

Nanofibers have been broadly researched and implemented in a variety of applications in the biomedical community, such as tissue engineering,[1] drug delivery,[2] and wound healing.[3] The explosion of research involving nanofiber-based scaffolds results from a structure that inherently mimics the extracellular matrix and a geometry that provides a high surface area to volume ratio.[4,5] When used for tissue engineering, their highly porous nature leads to a high influx of nutrients and yields improved cell growth and proliferation when compared to fibers of larger dimensions.[6] To facilitate the healing process, the scaffold properties must be tuned toward specific tissues. First, the bulk mechanical properties of the scaffolds must match that of the native tissue.[7] Mechanical properties of tissues can range from 10 kPa in muscle tissue to 1 MPa in cartilage to 10 GPa in bone.[8] Additionally, the degradation rate of a scaffold needs to match the regeneration rate of the targeted tissue, and the polymeric scaffold must maintain mechanical properties until sufficient regrowth occurs.[7] Moreover, because the regeneration rate *in vivo* varies widely, where stomach cells renew in 2−9 days, epidermis cells require 10−30 days, and osteoblasts require ∼6 months, tunable degradation rates are also needed.[9]

To match these varying regeneration rates, aliphatic polyesters are viewed as appealing materials due to their range of degradation kinetics.[10] Furthermore, blending multiple polyesters with different properties can yield materials that can be tuned.[11] *In vivo*, polyesters are susceptible to passive hydrolysis and enzymatic hydrolysis, which are both a two-step bulk erosion process (Figure 1).[12−14] (1) Aqueous media diffuse throughout the bulk of a material, and this rate is dependent on material properties such as molecular weight, crystallinity, phase separation, processing, and surface area. Consequently, manipulation of these properties has been explored to influence the overall degradation rate.[15] (2) Chain scission events occur at the labile ester linkages. These two steps in hydrolysis will first change the bulk mechanical properties, and once chain scission events occur on a large scale, weight loss can be measured. The final step of hydrolysis, weight loss, is often accompanied by a significant reduction in mechanical properties. To influence the rate of diffusion and chain scission, crystallinity and phase separation, both contributing factors in chain mobility, have been manipulated to tune the degradation rate. For example, an *in vitro* degradation study of polyester−peptide copolymers revealed that a high crystalline content played a more important role in the degradation rate relative to the hydrophobic content.[16] Additionally, Gaona et al. examined a blend of poly(lactic acid) (PLA) and poly(ε-caprolactone) (PCL) *in vitro* that phase

Received: April 13, 2021
Accepted: July 2, 2021
Published: July 19, 2021

ACS Publications © 2021 American Chemical Society

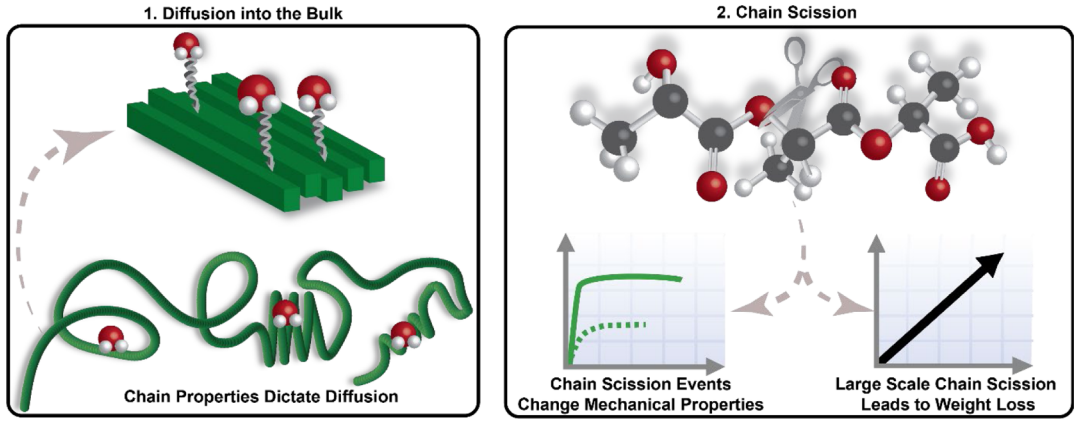

Figure 1. Schematic diagram of the hydrolytic degradation of polyester nanofibers. (1) Diffusion of the media into the bulk material is the initial step and the rate-limiting step. Several characteristics dictate the diffusion time, such as chain mobility, thickness, surface area, hydrophobicity, and molecular weight. Chain mobility is affected by confinement effects as well as crystalline content. The crystallite size also plays a role because larger crystallites restrict mobility. (2) Random chain scission events occur at the labile ester linkage in the backbone. The mechanical properties change once the chain scission events occur due to reductions in the molecular weight and/or changes in the crystalline region. Measurable weight loss is the last event to occur in hydrolysis and is typically an indicator of large-scale chain scission events.

separated, whereby the phase domain size was dictated by the formulation.[17] One formulation exhibited domain sizes that allowed both components of the blend to degrade at equal rates such that the initial blend composition was maintained, even though PLA typically degrades much more rapidly than PCL. It was found that the consistent blend composition allowed for sustained mechanics throughout the degradation process.

It is these two polyesters, PLA and PCL, that are the subject of intense study for biodegradable scaffolds because these semicrystalline polymers can easily be manipulated to fit precise specifications for a multitude of applications.[18,19] PLA has been deemed an excellent option to form the base of a biodegradable device due to the strong mechanical properties often observed, the potential for sourcing from a renewable feedstock, and the rapid degradation rate, where a naturally occurring metabolite is the byproduct.[20,21] However, PLA [glass transition temperature (T_g) of 60 °C] often is too brittle for certain applications.[21,22] Unlike glassy PLA, PCL has a flexible backbone that yields a low T_g (−60 °C) and high extensibility/toughness. However, the backbone structure of PCL lends the material to be highly hydrophobic, with a slow degradation rate.[23] Because of these opposing characteristics, many previous works have blended PLA and PCL as components of a fibrous scaffold such that the bulk material properties can be easily manipulated.[21,24−27]

Laboratory-scale nanofibers are often processed via electrospinning for use in biomedical applications. Electrospinning has a broad and historical usage because it utilizes a simplistic setup and has a minimal expense.[28] However, it is a solvent-based method that can be dramatically impacted by environmental influences such as temperature and humidity and has a low manufacturing throughput.[2] Consequently, other nanofiber fabrication methods have been sought. Previously, we have demonstrated the tunability of utilizing a scalable and melt-based fiber fabrication method, multilayer coextrusion.[6,29−33] This processing method coextrudes two (or more) immiscible polymers such that a composite tape is produced, in which nanofibers are embedded in a sacrificial matrix (Figure 2).[29] Because multilayer coextrusion is a melt-based process, no solvent is required, batch-to-batch variability

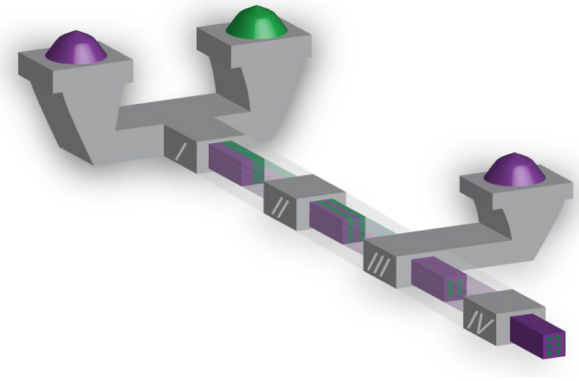

Figure 2. Schematic diagram of melt coextrusion. An overview of the process of multilayer coextrusion to fabricate a composite tape where a sacrificial polymer (purple) forms a matrix around nanofibers (green). This extrusion method comprised four major steps. Here, two immiscible polymers are fed into the extruder and vertically stacked such that their flows are adjacent to one another (step I). Then, these stacked melts pass through a series of vertical multipliers (step II). After step II, a skinning layer is applied to the top and bottom (step III). The melt then passes through a series of horizontal multiplication steps (step IV). Finally, the composite tape is passed through a die and the extrudate is collected.

is reduced, and the high throughput allows for the production of multiple kilograms per hour. Additionally, because this process fabricates rectangular fibers, a higher surface area to volume ratio is achieved when compared to cylindrical fibers.[6] These unique fibers have been covalently modified with biologically active molecules,[6,32,33] mechanically enhanced via post extrusion drawing,[30] and fabricated from several polyester blends.[29]

In our most recent multilayer coextrusion demonstration, we blended PLA and PCL to fabricate fibers with mechanical properties that could be tuned.[29] During this investigation of nonwoven fibers, we found that the blending process had distinct consequences on the crystalline region in both the PLA and PCL components. These outcomes were due to the blend morphologies inducing chain confinement into small domains within the nanofibers. Subsequently, the crystallinity

https://doi.org/10.1021/acsapm.1c00454
ACS Appl. Polym. Mater. 2021, 3, 3878−3890

in both components was depressed, and the mean size of individual crystallites was also influenced. PCL acted as a nucleation site for PLA, leading to the formation of larger PLA crystallites with increasing PCL content. However, because PLA has a higher crystallization temperature than PCL, the mobility of PCL was restricted after PLA crystallization. As a result, increased amounts of PLA caused a decrease in the mean crystallite size in the PCL component.

The spatial separation of the PLA and PCL components induced by the multilayer coextrusion process dictated the crystallization behavior of the fiber blends. We hypothesized that the diffusion rate of extruded PLA/PCL blended fibers in surrounding media would also be influenced, likely impacting the degradation rate relative to known fiber fabrication methods. Here, a continuum of PLA/PCL blended fibers, along with control PLA and PCL fibers, was examined during a four weeklong *in vitro* hydrolytic degradation study. While many *in vitro* and *in vivo* studies focus on properties such as the weight loss and the dispersity of polymer chains, this work focused on the impact of morphology, imparted by phase separation and processing, on the degradation rate as it pertains to nonwoven fiber mats acting as a functional material (i.e., suitable mechanical properties). In this study, we systematically discuss and highlight which aspects had the most significant contribution to the degradation profile of PLA/PCL nonwoven fibers. These findings not only further the technological impact of multilayer coextruded fibers but also add to the understanding of manipulating and predicting mechanical properties of biomedical nanofibers throughout the lifetime of their use.

EXPERIMENTAL SECTION

Composite Tape Fabrication. To fabricate the polyester/poly(ethylene oxide) (PEO) composite tapes, two different polyesters and two grades of PEO were obtained. PCL was acquired from The Perstorp Group (CAPA 6800, 87 kg/mol), and Nature Works provided PLA (INGEO BIOPOLYMER 2003D, 155 kg/mol).[34] To fabricate the polyester blends, PLA and PCL were mixed into three different formulations of 75 PLA/25 PCL, 50 PLA/50 PCL, and 25 PLA/75 PCL by weight percent (wt %). The blend formulations were fed into a corotating twin-screw extruder (W & P 25k-30) that had a screw length to diameter ratio of 28.5 and was set to 160 °C. The blended filaments were then pelletized. The PEO matrix component of the composite tape was then compounded. The PEO formulation was comprised of two PEO powders (100 and 200 kg/mol), mixed at a weight ratio of 70:30 (POLYOX WSRN-10:POLYOX WSN-80), and this mixture was melt blended and pelletized under the same conditions as the PLA/PCL formulations. This PEO blending step was critical to ensure that the viscosity of PEO matched that of the PLA/PCL component during the multilayer coextrusion process.[35] Additionally, prior to each extrusion step, materials were dried under vacuum for 48 h at 40 °C.

The multilayer coextruder was outfitted with 16 vertical multipliers, an additional hopper that allows for a 33% by volume skin layer of the PEO matrix, and 4 horizontal multipliers. The materials were again dried for 48 h at 40 °C under vacuum and then fed into the multilayer coextruder. The temperature was set to 200 °C so that each component had a matching viscosity. Additionally, the extruders that fed in the PEO and PLA/PCL pellets were set to a 1:1 pump ratio, and the polymer melts were forced through a 1 inch tape die. An equilibration period of 25 min was allowed before the materials were collected to ensure that a uniform pressure was achieved. Here, the systems formed a continuous composite tape such that 1024 individual, rectangular, PLA/PCL fiber domains were embedded in a PEO matrix. Once the tapes were ejected through the die, they were collected onto a chilled steel roller rotating at 30 rotations per minute (rpm). The tapes were subsequently placed onto a conveyer belt.

Fiber Isolation. To isolate the fibers, a three-step wash-delamination-wash process was implemented. This procedure has previously been optimized such that a minimum of 89.9% of the PLA/PCL weight content was achieved.[29] During this process, the PEO matrix was dissolved, and the PLA/PCL nonwoven fiber mats were left unchanged. Proton nuclear magnetic resonance (^{1}H NMR, 600 MHz) spectroscopy was used to ensure that PEO removal was successful. In preparation for ^{1}H NMR, PLA/PCL nonwoven fiber mats were dissolved in deuterated chloroform ($CDCl_3$). The relative weight fraction of the PLA/PCL component was calculated using single, isolated peaks characteristic of PEO (3.7 ppm), PLA (5.1 ppm), and PCL (4.1 ppm) (eq S11).

***In Vitro* Degradation.** To probe the *in vitro* degradation profile of bioresorbable PLA/PCL nonwoven fiber mats, a hydrolytic degradation experiment that mimicked *in vivo* conditions was conducted. During this degradation study, the PLA/PCL fibers were exposed to physiological conditions for a duration of four weeks. The mats were placed into 20 mL scintillation vials and were fully immersed in PBS solution (Fisher Scientific) with a pH of 7.4. The degradation vessels were then placed in an oven that was set to 37 °C. The buffer solution was replaced each week, and the degradation periods of interest were one, two, three, and four weeks. At each point of interest, the nonwoven PLA/PCL fiber mats were removed from the vials, washed thoroughly with methanol, and left to dry overnight. Once dry, the fibers were tested for fiber integrity, weight loss, blend composition, crystallinity size/amount, and mechanical analysis.

Fiber Integrity. To investigate the fiber architecture or integrity, nonwoven PLA/PCL fiber mats were imaged via SEM (Jeol JSM-7400F). Prior to fiber submersion as well as at each time point, the nonwoven fibers were mounted on a sample stage that was sputter-coated with a thin layer of Au/Pd. SEM was then conducted at an accelerating voltage of 3 kV.

Weight Loss. Three nonwoven samples of each fiber type were weighed prior to the *in vitro* degradation process. The samples had dimensions of 5 mm by 10 mm and weighed ∼15 mg. After each week, the samples were removed from the PBS solution and generously washed with methanol and distilled water. The nonwoven PLA/PCL fibers were then allowed to dry overnight, and the following day, each sample was weighed. The percent (%) weight loss (eq 1) was calculated using the following equation

$$\text{weight loss (\%)} = \frac{(W_i - W_x)}{W_i} * 100 \quad (1)$$

where W_i is the weight prior to the fiber submersion and W_x is the weight of the dried fibers at the specified time points.[9] After determining W_x, the dried fibers were returned to the buffer media. Additionally, blended PLA/PCL samples with measurable weight loss were characterized further by ^{1}H NMR to determine the weight fraction of PLA within the blended nonwoven fiber systems (eq S16).

Crystallinity. Two characterization methods were utilized to examine the crystalline domains of the PLA/PCL nonwoven fibers: dynamic scanning calorimetry (DSC, TA Discovery Series) and wide-angle X-ray scattering (WAXS, Xenocs Xeuss 2.0). DSC was conducted in triplicate to characterize the relative amount of crystalline versus amorphous regions; WAXS was utilized to quantify the mean crystallite size. For DSC studies, each sample set was tested in sealed, hermetic pans where a blank pan was used as a reference, all under a nitrogen atmosphere. The samples were initially cooled and held at 0 °C for 3 min and then heated to 200 °C at a rate of 10 °C/min. Then, the PLA/PCL nonwoven fiber mats were cooled back down to 0 °C at a rate of 10 °C/min. The enthalpy of melting was then measured using TA Instrument software, Trios.

WAXS was carried out to probe the mean crystallite size using Xenocs Xeuss 2.0. The detector was a charge-coupled device with a pixel resolution of 486 × 619 (1 pixel—0.172 cm). X-rays were generated at 50 kV at a wavelength of 1.542 Å. The mounted PLA/PCL mats were exposed to the X-ray source for 15 min, where the

https://doi.org/10.1021/acsapm.1c00454
ACS Appl. Polym. Mater. 2021, 3, 3878−3890

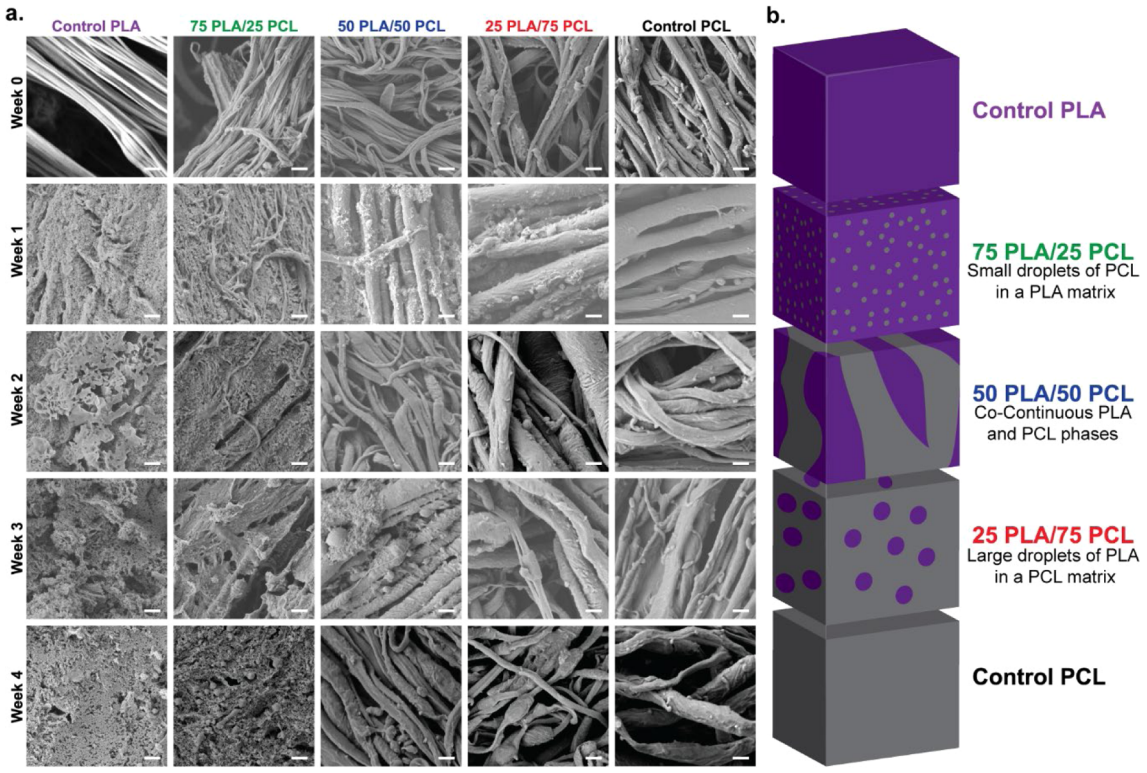

Figure 3. Morphology of blended fibers during degradation. (a) SEM micrographs obtained at 10,000× magnification with a scale bar of 1 μm of PLA/PCL nonwoven fiber mats at weeks zero, one, two, three, and four. Initially, fibers were calculated to be ~300 nm in width and 200 nm in thickness. The change in the fiber architecture was analyzed for each PLA/PCL fiber system through the duration of the degradation study. (b) Previously reported morphology of each PLA/PCL nonwoven fiber blend depicted in a single schematic. Moving from top to bottom, the PCL content is increased. The 75 PLA/25 PCL blends were found to have small PCL droplets in a PLA matrix, the 50 PLA/50 PCL blends were observed to be co-continuous, and the 25 PLA/75 PCL blends were made up of large PLA droplets in a PCL matrix.

sample-to-detector distance was set to 800 cm. The instrument was calibrated with silver behenate, and all spectra were corrected for background noise. To obtain intensity as a function of the scattering vector, q, azimuthal averaging was performed. The peaks were then processed via Origin 8.1, where they were fit using a Lorentzian function. Individual WAXS peaks were fit to determine the full width at half-maximum (FWHM) to calculate the mean crystallite size (L_{hkl}) (eq 2) using the Scherrer formula[36]

$$L_{hkl} = \frac{K\lambda}{B_{hkl} \cos \theta_{hkl}} \quad (2)$$

where L_{hkl} was correlated to a shape factor (K, typically 0.89 for polymers) the wavelength (λ), FWHM (B_{hkl}), and the Bragg angle (θ) for the reflection of interest.

Tensile Testing. The porosity of the PLA/PCL nonwoven fibers was found by calculating the void fraction (eq S19), and the cross-sectional area was corrected according to the measured porosity. The nonwoven fibers of similar length (~15 mm) were loaded between Teflon clamps of a Zwick/Roell mechanical testing instrument. Tensile testing was performed at room temperature at a rate of 50% min^{-1}. A minimum of five samples per PLA/PCL blend type were tested. Using Origin 8.1, the stress and strain at the yield point were determined, and the modulus was calculated by applying a linear fit at 2% strain.

RESULTS

Microscale Degradation Fiber Integrity and Morphology. Prior to the *in vitro* degradation process, composite tapes, where PLA/PCL fibers were encased in a PEO matrix, were extruded via multilayer coextrusion, with results consistent with those previously reported.[29] During this process, three blends were formulated (75/25, 50/50, and 25/75 PLA/PCL). These blends and two controls (PLA and PCL) were used as the fibrous component of the composite tape, and PEO formed the sacrificial matrix. The tapes for each system were collected, and the PLA/PCL fibers were isolated and delaminated from the matrix to form nonwoven fiber mats (Figure S1). The polyester weight content was 89.9% or greater, as confirmed by ^{1}H NMR (Figure S2). Additionally, the fiber mats were imaged via SEM to determine individual fiber dimensions prior to the degradation study (Figure 3a). Each PLA/PCL system was calculated to be ~300 nm in width and ~200 nm in thickness (Figure S3, Table S4). In a recent publication, we detailed the morphologies of these blended nanofiber systems using selective solvent etching in tandem with SEM.[29] The depictions shown in Figure 3b are scaled to represent these microstructural features and are useful for the interpretation of the degradation results. Distinct morphologies were observed within each of the three PLA/PCL blends: small droplets (~50 nm) of PCL were encased in a PLA matrix in the 75 PLA/25 PCL blend, a co-continuous morphology was observed in the 50 PLA/50 PCL blend, and large droplets (~100 nm) of PLA were dispersed in a PCL matrix in the 25 PLA/75 PCL blend. After the fibers were characterized, the PLA/PCL nonwoven fibers were placed in aqueous conditions that were meant to mimic physiological conditions. Here, fibers were submerged in PBS (pH 7.4) at 37 °C. After one, two, three, and four weeks, the PLA/PCL fiber mats were removed from the solution and thoroughly washed with methanol. The washed and dried mats were first imaged via SEM to understand the

https://doi.org/10.1021/acsapm.1c00454
ACS Appl. Polym. Mater. 2021, 3, 3878−3890

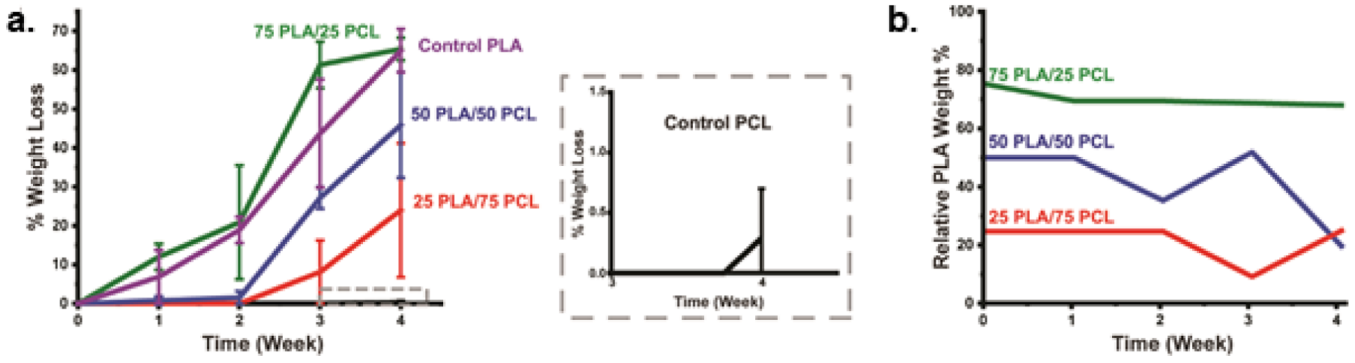

Figure 4. Degradation kinetics. (a) Weight loss of each PLA/PCL nonwoven fiber system tracked over a four weeklong study to understand the macroscopic changes in each fiber system that resulted from hydrolysis. (b) Relative wt % of PLA evaluated to calculate the blend composition throughout the degradation study when measurable weight loss was observed.

hydrolytic effects on the fibrous architecture. The collected micrographs indicated that the fiber integrity and fiber size varied during the four weeklong study. For example, the control PLA fiber mats were observed to lose the integrity of their fibrous architecture after the first week, and the control PCL fibers were able to maintain their fibrous shape throughout the entire study. However, the PCL fibers were noticeably swollen, which is commonly observed in PCL systems.[37,38] Similar to the PLA control system, the 75 PLA/25 PCL nonwoven fibers lost nearly all fibrous morphology after week one. A minimal fraction of the system resembled fibers until the week two time point, and thereafter, the fiber integrity was completely lost. Once PCL composed half of the fibrous system, the 50 PLA/50 PCL nonwoven fibers maintained a fibrous architecture. While they remained fibrous in overall shape, surface roughening was apparent after the week one time point, indicating that the 50 PLA/50 PCL fiber mats were not as uniform in size, shape, or appearance. Similarly, the 25 PLA/75 PCL system also maintained a fibrous architecture for the entirety of the study, but the 25 PLA/75 PCL fibers experienced limited erosion of the smooth surface. These findings indicated that the physical effect on the microstructure of the nonwoven PLA/PCL fibers was heavily influenced by the composition of the blend. Because PCL is highly hydrophobic, it has been known to act as a hydrophobic "shield" when blended with a more hydrophilic material.[39] This "shield" can delay the diffusion of the media into the bulk and increase the longevity of the material properties. Consequently, when blends were formulated with at least 50 wt % PCL, properties, such as the fiber architecture, were maintained.

Macroscale Degradation—Weight Loss and Blend Composition. Once the microscale and morphological effects were confirmed, large-scale chain scission events were detected through weight loss calculations for the PLA/PCL nonwoven fiber mats throughout the four weeklong study (Figures S2–S6, 4a). Furthermore, ^{1}H NMR was utilized to determine the composition of the blends to determine which component was the source of the weight loss (Tables S2–S4, Figure 4b). These values are represented as a relative percentage to demonstrate how degradation kinetics impacted each polymer within the blend. An important fact is that weight loss is the final step a material experiences during hydrolysis. Consequently, when weight loss was detected, it was assumed that media had previously diffused throughout the bulk of the material and successfully initiated large-scale chain scission events. During this study, PLA mats immediately and steadily exhibited weight loss, and a final loss of 64.9% ± 5.6 wt % was measured. In contrast, the control PCL nonwoven fibers were measured to have almost no weight loss for the duration of the experiment (0.29% ± 0.29 wt % at week four). Because PCL is more hydrophobic, it was anticipated that the trends in weight loss for the blended PLA/PCL nonwoven fibers would primarily depend on the blend composition. Correspondingly, the 75 PLA/25 PCL system initially appeared to follow the same trend as the control PLA nonwoven fibers. Here, an initial weight loss was measured at the week one time point, and continual weight loss was observed, where a total weight loss of 65.4% ± 6.4 was measured. While the 75 PLA/25 PCL fibers appeared to follow the same trend as the control nanofibers, the relative PLA wt % measured at each time point suggested that the 75 PLA/25 PCL blended system degraded differently than the PLA control. Interestingly, the relative PLA wt % was consistent throughout the four weeks. The blend composition data suggested that both the PLA and the PCL components experienced large-scale chain scission events. If only the PLA component contributed to weight loss, the relative PLA wt % would have decreased. The consistency of the composition of the 75 PLA/25 PCL system is significant because the control PCL system had no weight loss until the final week, where less than 0.3% weight loss was recorded. Because the 75 PLA/25 PCL system had a total weight loss of 65.4%, and 25% of the total was lost within the PCL component, it can be calculated that ∼16 wt % of the PCL component was lost during the four weeklong study. This PCL weight loss varies greatly from the negligible weight loss observed in the control PCL system. This variance is likely due to the phase-separated morphology of the system. Specifically, the domain size of the PCL droplets may have allowed the two components of the blend to degrade at a consistent rate, which is only possible when PCL domain sizes are submicrometer.[17] In addition, the 50 PLA/50 PCL nonwoven fibers initially followed the expected composition-based weight loss trend, where weight loss was delayed, compared to the 75 PLA/25 PCL blend. The total weight loss (45.9% ± 13.6) of the 50 PLA/50 PCL system was less than that of the 75 PLA/25 PCL system. The delay in weight loss from week one to week two is attributed to the increase in the PCL content with PCL functioning as a hydrophobic shield and decreasing the diffusion rate of the aqueous media. The initial weight loss time point included a decrease in relative weight % of PLA. However, at the following time point (week three), the increase in weight loss was measured along with an

https://doi.org/10.1021/acsapm.1c00454
ACS Appl. Polym. Mater. 2021, 3, 3878−3890

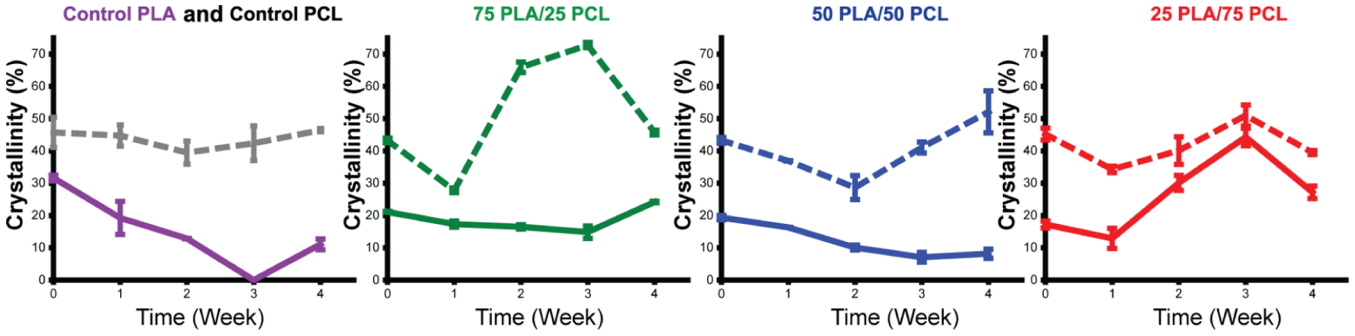

Figure 5. Crystallinity (%). The melting enthalpy, as measured via DSC, of both the PLA and PCL components was tracked throughout the study to examine the effects of hydrolysis in the crystalline region (PLA: solid line and PCL: dashed line).

increase in relative wt % of PLA. We interpret this to mean that PCL was the component primarily affected by the large-scale chain scission events. The increase in PCL degradation time, compared to the control, is likely due to the blending of PCL with a more hydrophilic polymer, such as PLA, that allowed for more rapid diffusion of the aqueous media.[39] However, an increase in PLA wt % was not observed at the final time point. Similarly, the 25 PLA/75 PCL nonwoven fiber system was found to have a complex timeline for the large-scale chain scission events. Again, the increase in the PCL component further delayed the initial weight loss time point to week three. Additionally, the initial weight loss time point also had a decrease in relative wt % of PLA. However, at the final time point, there was an increase in relative wt % of PLA. As with the 50 PLA/50 PCL system, this increase is likely due to the addition of the more hydrophilic PLA component, which increased the diffusion rate of the media.[39]

Crystalline Fraction and Crystallite Size. The characteristics of the crystalline region significantly impact the rate of degradation and are dependent on the manufacturing method.[40,41] After probing the hydrolytic effects on the macrostructure of the PLA/PCL nonwoven fibers, the crystalline regions were examined to determine which component of the blends was affected by hydrolysis throughout the time course of the study (PLA, PCL, crystalline, or amorphous). Initially, DSC was utilized to examine the changes in percent crystallinity to determine if the ratio of crystalline to amorphous fraction changes after each time point (Figures 5, S4). Here, samples were run in triplicate at a heating rate of 10 °C/min. Because thermal history was dictated by the multilayer coextrusion process, the first heating cycle was utilized for characterization. The melting enthalpy was then measured using Trios software by integrating the melting transition. In the control PLA system, a rapid decrease in crystallinity was measured until there was no melting enthalpy that was not correlated to cold crystallization observed at the week three time point. However, a melting enthalpy was observed during the final time point. The disappearance and re-emergence of the endothermic phase transition indicates that hydrolysis could occur in the crystalline region to completely erode the crystalline phase. At the week four time point, recrystallization is assumed to have occurred. Many studies regarding polyester crystallization, primarily using PLA, highlight that an increase in the crystallinity measured through DSC during hydrolysis is a result of the recrystallization of small chain fragments.[17] Using this framework, we conclude that a similar mechanism is responsible for the thermal behavior of the control PLA fibers. In contrast to the PLA control, very little change in the crystallinity was measured in the control PCL fiber system. The consistency in the crystallinity indicates that the same energy is required to melt the crystalline region throughout the duration of the study, meaning little crystallinity was lost or gained due to hydrolysis. Additionally, it is likely that the amorphous regions also were relatively unaffected because the melting enthalpy did not significantly increase.[42]

While the controls demonstrated uncomplicated trends (rapid loss of PLA crystallinity and consistent crystallinity in PCL), the blended PLA/PCL nonwoven fibers exhibited a more dynamic degradation progression. To understand the complexities thoroughly within the blended PLA/PCL nonwoven fibers, the crystallinity of both the PLA and PCL components was calculated separately. When examining macroscopic hydrolysis changes, the 75 PLA/25 PCL nonwoven system closely mimicked the control PLA system. However, differences emerge after the effects within the crystalline domain were observed. For example, while a slight decrease in percent crystallinity in the PLA component of the 75 PLA/25 PCL system was measured for the initial three weeks, the downward trend is much less severe than the loss observed in the control PLA system. Yet, the two systems are similar in that there is an increase in PLA crystallinity at the final time point. Considering the PCL component of the 75 PLA/25 PCL system, while an initial decrease in the melting enthalpy was measured at two consecutive time points, a final decrease was observed at week four. This final time point was comparable to the initial percent crystallinity of PCL. Intriguingly, when the PCL content of the blend was increased to 50 PLA/50 PCL, a similar PCL trend is observed, where an initial decrease is followed by an increase, and the final crystallinity is equivalent to the initial value measured. However, the 50 PLA/50 PCL system displays a different PLA trend. Here, a steady decrease in the percent crystallinity in the PLA component was measured for the entirety of the study. Increasing the PCL content to 25 PLA/75 PCL produced another unique trend for the enthalpy in the PLA component. Here, the crystallinity of PLA was relatively consistent throughout the study. Additionally, similar trend behavior of the PCL component was observed, where the 25 PLA/75 PCL system exhibited an initial decrease, followed by two weeks of increase. The initial decrease in both components suggested that degradation occurred in the crystalline fraction and the subsequent increase indicated degradation in the amorphous content.

A noteworthy phenomenon in each PLA/PCL nonwoven fiber system was that almost every component was measured to

https://doi.org/10.1021/acsapm.1c00454
ACS Appl. Polym. Mater. 2021, 3, 3878−3890

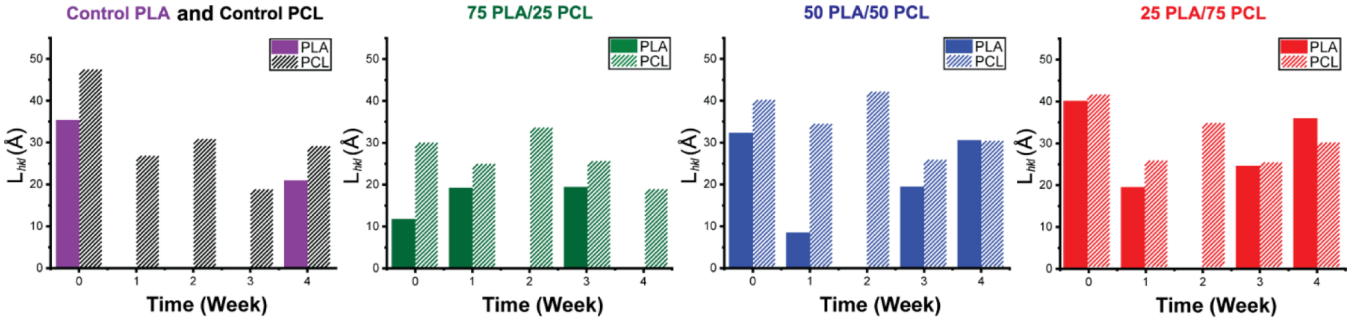

Figure 6. Crystallite sizes for fibers during degradation. WAXS was conducted to confirm recrystallization and to track the mean crystallite sizes for two reflections (110)/(200) and (110) that correspond to PLA and PCL, respectively.

have an initial decrease in percent crystallinity. These reductions are important because, for typical semicrystalline polyester materials undergoing hydrolysis, increases in the melting enthalpy are expected as diffusion into the less tightly packed amorphous regions is expected to be more rapid than diffusion into the crystalline regions.[43] As a result, chain scission events occur initially in the amorphous region, and the ratio of crystalline to amorphous content is increased; thus, comparatively, higher energy is required to melt the crystallites.[42] However, there are factors that could explain the initial decrease in crystallinity: (1) The PLA component, which is less hydrophobic than PCL, contains a higher concentration of labile ester linkages. Additionally, nanofibers are highly porous, allowing for more rapid diffusion into the bulk; it is likely that the week one time point was too late to measure the initial effects of hydrolysis for PLA.[12] (2) Semicrystalline polymers are known to have rigid amorphous regions that can affect the rate of diffusion into the amorphous regions.[12,44,45] Within these rigid regions, the amorphous content does not have typical mobility because it is either constrained due to the material being highly crystalline or phase confinement factors (i.e., immiscible blend morphologies). As measured in our previous work with extruded PLA/PCL nonwoven fibers, control PCL fibers were measured to have a crystalline fraction of 46% ± 2.[29] Consequently, the highly crystalline nature of the PCL fibers confined the amorphous content such that it served as a rigid amorphous region. Additionally, because the semicrystalline polymer chains experienced confinement effects due to processing conditions forcing the PLA/PCL melts into a nanofiber architecture as well as the spatial separation between the PLA/PCL components, it is likely that the blended nonwoven systems also experienced a rigid amorphous region phenomenon.[45] The rigid amorphous region has previously been observed to cause the crystalline region to degrade before the amorphous fraction in a PCL system.[12] A rigid amorphous fraction in a PLA system was also observed in an immiscible blend of PLA/poly(hydroxybutyrate).[46] Sajkiewicz et al. determined *in vivo* that the presence of a rigid amorphous fraction caused hydrolysis to occur initially in the crystalline region of PCL, rather than in the amorphous fraction.[12]

To confirm recrystallization and measure the mean crystallite size (L_{hkl}) of the PLA and PCL domains, we employed WAXS to characterize the degraded PLA/PCL fibers.[17,47,48] WAXS was utilized to obtain the L_{hkl} of the two isolated crystal reflections, (110)/(200) and (110), that correspond to PLA and PCL, respectively (Figures 6 and S5).[28] Additionally, these two reflections were the most dominant crystal reflections for the respective polyesters. To obtain L_{hkl}, the 1D WAXS patterns were fit with a Lorentzian fit, and the FWHM values calculated for the two crystal reflections were substituted into eq 2. It was expected that the L_{hkl} values would decrease throughout the hydrolytic process due to chain scission events occurring and erode the crystalline domains.[12] During the early time points, this trend was observed within the control PLA and PCL nonwoven systems. Initially, in the PLA control, the (110)/(200) reflection was observed to form crystallites of 35.3 Å prior to the degradation. After the initial time point, the (110)/(200) reflection was not present. However, the (110)/(200) reflection re-emerged at the final time point, week four, and it was calculated to be 20.9 Å. This re-emergence suggested that small PLA chain fragments recrystallized between week three and week four. Furthermore, an endothermic phase transition was observed in DSC for the control PLA system during week two. This melting transition is likely caused by other crystal reflections, not the (110)/(200) reflection, but these reflections occur at a similar q as PCL-specific reflections (Figure S6). We only focused on the (110)/(200) reflection for PLA as it is the only PLA reflection that is isolated from the PCL crystal reflections. While PLA has been cited as undergoing recrystallization in the literature, PCL is not reported to exhibit this phenomenon.[17]

A 47.5 Å crystallite was initially calculated for the control PCL (110) crystal reflection. While the crystallite size generally decreased over the first three weeks, a noticeable increase from week three to week four (18.9 to 29.2 Å) was measured in the PCL control. This increase in size could be an indication of fragmented PCL chains experiencing recrystallization. However, it is more likely that the experimental conditions led to annealing of the control PCL system due to exposure to an environment well above the T_g for several weeks and aqueous media induced a plasticization effect.[49,50]

Within the blends, an interesting trend of the mean crystallite size emerged. While it was initially believed that the smallest crystallites would be the first to be degraded, other factors such as morphological confinement played a larger role in the degradation process. While the 75 PLA/25 PCL nonwoven fiber system was found to have the smallest initial PLA mean crystallite (11.5 Å), there was no change after the initial week. However, the 50 PLA/50 PCL (32 Å) and the 25 PLA/75 PLA (39 Å) nonwoven fiber mats displayed larger initial PLA crystallites, and both mats experienced a reduction in size (32−8 Å and 39−19 Å, respectively). The reduction in the PLA mean crystallite size was likely due to the previously measured, larger PLA crystallites restricting mobility in an amorphous domain. Consequently, the restricted mobility

https://doi.org/10.1021/acsapm.1c00454
ACS Appl. Polym. Mater. 2021, 3, 3878−3890

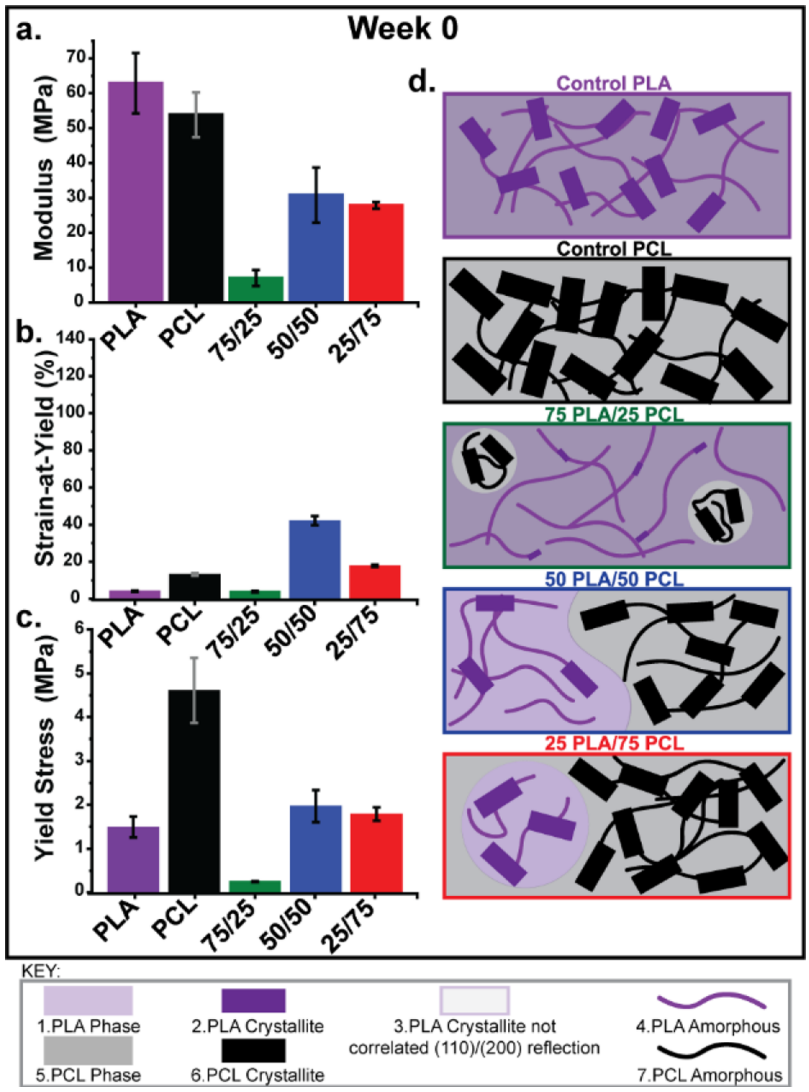

Figure 7. Mechanical properties prior to degradation. Values measured by tensile testing (a) Young's modulus, (b) strain-at-yield, and (c) yield stress. (d) Relative crystallite size and amount schematically drawn to visualize the structural differences between each system. In these schematics, the size and fraction of crystallites (depicted as blocks) were normalized to WAXS and DSC data to generate a realistic depiction of the microstructure (75/25 = 75 PLA/25 PCL, 50/50 = 50 PLA/50PCL, and 25/75 = 25 PLA/75 PCL).

allowed for a more rapid erosion of the PLA crystallites (i.e., rigid amorphous fraction effect). For all three systems, the (110)/(200) reflection was not apparent at week two, but the reflection was observed to reappear at the following time point (week three) in each of the systems. This reappearance indicated that the systems containing PLA were able to recrystallize. In the final week, the (110)/(200) reflection was no longer apparent in the 75 PLA/25 system, implying that the recrystallized region was readily degraded. However, in the other two fiber blends, 50 PLA/50 PCL and 25 PLA/75 PLA, not only was the (110)/(200) reflection apparent, the PLA crystallite size was found to increase from 19 to 30 Å in the 50 PLA/50 PCL system and from 24 to 35 Å in the 25 PLA/75 PCL system. The preservation and growth of the crystalline regions were likely due to additional small chain fragments recrystallizing, and the larger PCL component blends were able to delay the erosion time.

Unlike the PLA component, the PCL fraction in the blends maintained more stable crystallite sizes in each of the PLA/PCL fibers, where PCL crystallites were measured to decrease gradually throughout the study. Still, some subtle deviations were observed. For example, at the week two time point, the PCL mean crystallite size was observed to increase in the systems 75 PLA/25 PCL from 26 to 31 Å, 50 PLA/25 PCL from 34 to 42 Å, and 75 PLA/25 PCL from 25 to 34 Å. In all blended fiber systems, PCL is typically restricted by the PLA component due to morphological constraints. However, at week two, the (110)/(200) reflection was not detected. Therefore, it is reasonable to conclude that the disappearance of the dominant PLA crystallite afforded the PCL component more mobility and led to annealing.[49]

Mechanical Properties. After an examination of the hydrolytic effects on the macro- and microstructures of the PLA/PCL nonwoven fibers, the mechanical properties were investigated (Figure S7). Based on the measured values and structural characteristics observed, the effect of morphology (chain mobility and crystallinity) and blend composition on the ability of each system to maintain robust mechanics during hydrolytic degradation was explored. Similar to our previous mechanical analysis, the initial mechanical properties were

https://doi.org/10.1021/acsapm.1c00454
ACS Appl. Polym. Mater. 2021, 3, 3878−3890

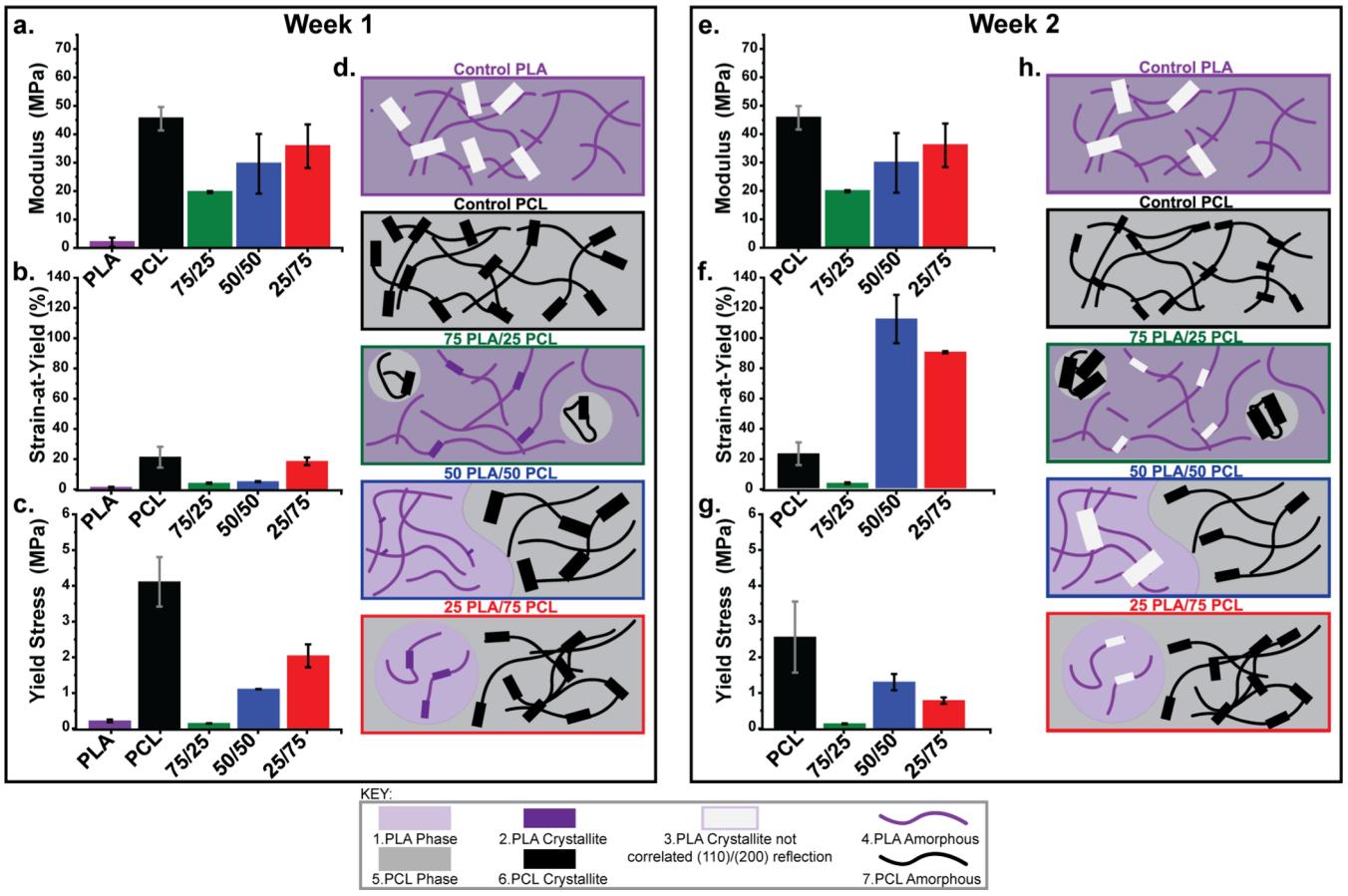

Figure 8. Mechanical properties at weeks one and two. Week one: mechanical properties one week after degradation. Values were measured by tensile testing (a) Young's modulus, (b) strain-at-yield, and (c) yield stress. (d) Relative crystallite size and amount for the control PLA, control PCL, 75 PLA/25 PCL, 50 PLA/50 PCL, and 25 PLA/75 PCL schematically drawn to visualize the structural differences between each system. In these schematics, the size and fraction of crystallites (depicted as blocks) were normalized to WAXS and DSC data to generate a realistic depiction of the microstructure. Week two: mechanical properties two weeks after degradation. Values were measured by tensile testing (e) Young's modulus, (f) strain-at-yield, and (g) yield stress. (h) Relative crystallite size and amount for the control PLA, control PCL, 75 PLA/25 PCL, 50 PLA/50 PCL, and 25 PLA/75 PCL schematically drawn to visualize the structural differences between each system. In these schematics, the size and fraction of crystallites (depicted as blocks) were normalized to WAXS and DSC data to generate a realistic depiction of the microstructure (75/25 = 75 PLA/25 PCL, 50/50 = 50 PLA/50PCL, and 25/75 = 25 PLA/75 PCL).

reported, and structure−property connections were highlighted.[27,51] Initially, the control PLA fibers were strong with little extensibility (modulus of 62 MPa, yield stress of 1.5 MPa, and strain-at-yield of 4.1%) (Figure 7a−c). The strength of the control PLA system was likely influenced by the large crystallites, as well as the high melting enthalpy (Figure 7d).[52] The control PCL fibers had similar mechanical properties, where the modulus was 53 MPa (Figure 7a), yield stress was 4.6 MPa (Figure 7c), and strain-at-yield was 13% (Figure 7b). While PCL is typically seen as a rubbery-elastic-like material, the control PCL nonwoven fibers were found to have significant crystallinity and large crystallite sizes (Figure 7d), which led to a high modulus and yield stress.[51] Overall, the PLA/PCL blended fibers were measured to have poorer mechanical properties than expected due to unfavorable morphological constraints and reduced crystallinity (Figure 7d).[53,54] Still, informative structure−property relationships were observed. In the 75 PLA/25 PCL system, the PLA matrix was found to have drastically smaller PCL crystallites, compared to the other nonwoven fibers, and a low melting enthalpy for the PCL component was measured (Figure 7d). These aspects of the 75 PLA/25 PCL nonwoven fibers likely played a role in the low modulus (6.2 MPa) (Figure 7a), low strain-at-yield (3.9%) (Figure 7b), and low yield stress (0.2 MPa) (Figure 7c) measured. Interestingly, the 50 PLA/50 PCL system exhibited the highest mechanical properties compared to the other blend formulations (Figure 7a−c). Because the 50 PLA/50 PCL fibers exhibited a co-continuous morphology, the PCL and PLA domains were less restricted. While the PLA enthalpy of melting was lower than that of the 75 PLA/25 PCL blend, the PLA individual crystallites were much larger (Figure 7d). Additionally, a higher melting enthalpy in the PCL component was measured. Increasing the PCL component (25 PLA/75 PCL) led to mechanical properties that were similar to the 50 PLA/50 PCL system (Figure 7a−c). While the PCL melting enthalpy was higher in the 25 PLA/75 PCL system than in the 50 PLA/50 PCL system (Figure 7d), which is typically associated with a stronger material, the 25 PLA/75 PCL nonwoven fibers did not have enhanced mechanics. Here, morphology played a key role due to higher chain mobility under an applied force for co-continuous morphologies compared to droplet-in-matrix microstructures.[27]

https://doi.org/10.1021/acsapm.1c00454
ACS Appl. Polym. Mater. 2021, 3, 3878−3890

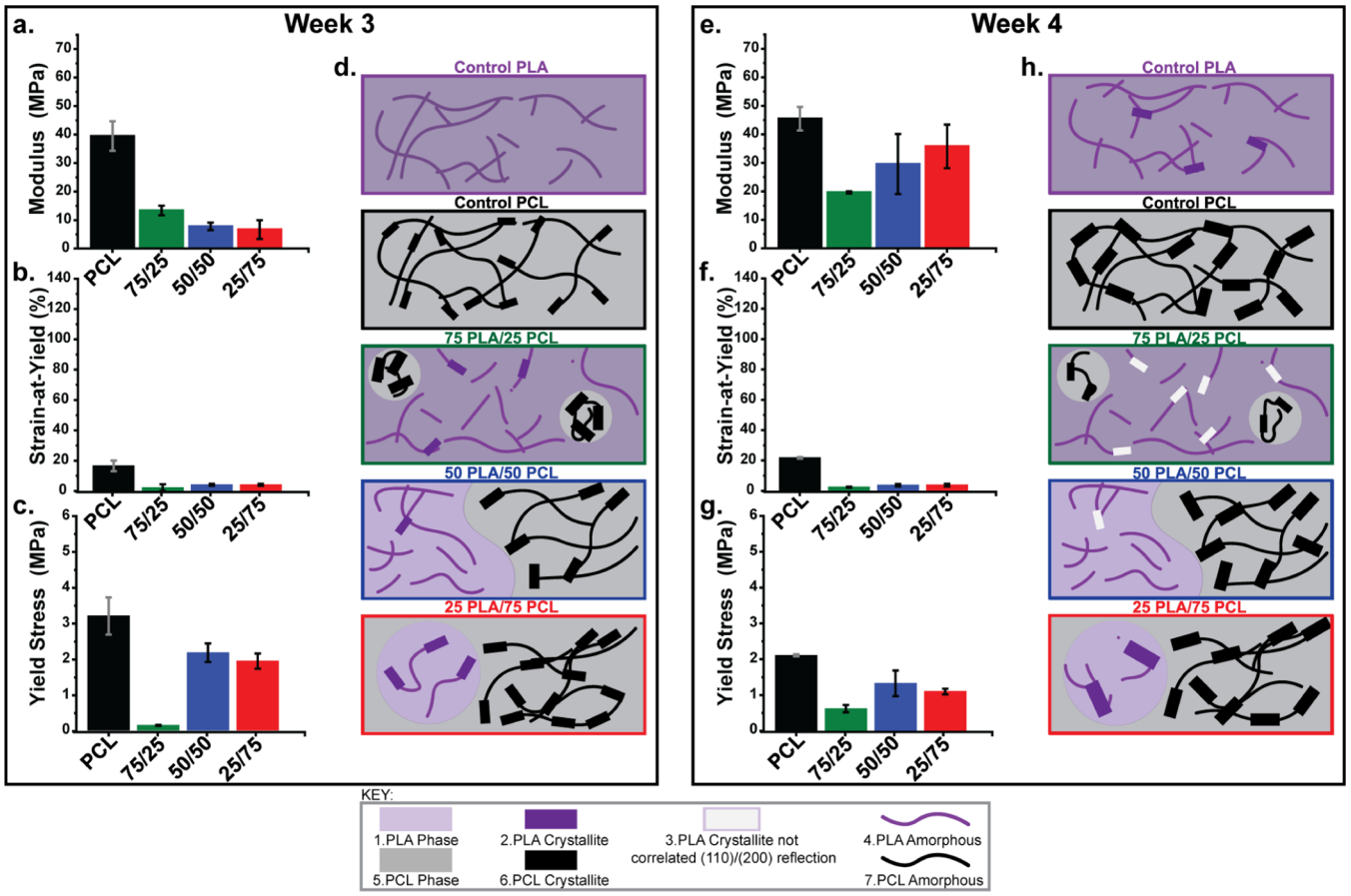

Figure 9. Mechanical properties at three and four weeks of degradation. Week three: mechanical properties three weeks after degradation. Values were measured by tensile testing (a) Young's modulus, (b) strain-at-yield, and (c) yield stress. (d) Relative crystallite size and amount for the control PLA, control PCL, 75 PLA/25 PCL, 50 PLA/50 PCL, and 25 PLA/75 PCL schematically drawn to visualize the structural differences between each system. Week four: mechanical properties four weeks after degradation. Values were measured by tensile testing (e) Young's modulus, (f) strain-at-yield, and (g) yield stress. (h) Relative crystallite size and amount for the control PLA, control PCL, 75 PLA/25 PCL, 50 PLA/50 PCL, and 25 PLA/75 PCL schematically drawn to visualize the structural differences between each system. In these schematics, the size and fraction of crystallites (depicted as blocks) were normalized to WAXS and DSC data to generate a realistic depiction of the microstructure (75/25 = 75 PLA/25 PCL, 50/50 = 50 PLA/50PCL, 25/75 = 25 PLA/75 PCL).

Once the nonwoven fibers were subjected to physiological conditions, drastic shifts in mechanical properties were observed (Figure 8a–c). After week one, the control PLA nonwoven fibers exhibited a decrease in each reported property likely due to the loss of the (110)/(200) crystal reflection, decrease in melt enthalpy (Figure 8d), and loss in mass. In contrast, only a slight change in the PCL crystallite size (Figure 8d) was observed in the control PCL system, and no significant change in mechanical properties was measured. More similar to the control PLA, the 75 PLA/25 PCL nonwoven fibers exhibited a decrease in each property but to a lesser extent than the reduced mechanical properties exhibited by the control (Figure 8a–c). The loss in melting enthalpy for both components of the blend as well as weight loss led to structural changes and did not allow for the initial properties to be maintained (Figure 7a–c). Even when the PCL content was increased to 50 PLA/50 PCL, structural changes were still found. The melting enthalpy was reduced in both components, and the PLA crystallites were significantly smaller (Figure 8d). Because of these changes in the crystalline region, the yield stress (Figure 8c) and strain-at-yield (Figure 8b) decreased. Once the PCL content was further increased to 25 PLA/75 PCL, the only structural change observed was a decrease in the PLA mean crystallite size (Figure 8d), but the mechanical properties were unaffected by this change. This connection suggested that the size of the crystallites in the minor stages of a blend plays a limited role in overall bulk mechanics.

The degradation studies continued to the two week time point, and important mechanical changes were observed. The control PLA nonwoven fibers were not feasible for mechanical testing because they were no longer structurally viable. Complete loss of mechanical strength occurred after only 20% weight loss. In contrast, only a shift in elasticity, where a lower modulus (Figure 8e) and yield stress (Figure 8g), but higher strain-at-yield (Figure 8f) was measured for the PCL control. This increase in the elastic behavior is likely the result of a decrease in the mean crystallite size (Figure 8h). The decrease in the crystallite size may have allowed for more chain mobility and generated a more elastic mechanical response behavior. Similar to an observation from week one, the 75 PLA/25 PCL nonwoven fiber properties were unchanged even though an increase in the PCL mean crystallite size and enthalpy of melting was observed (Figure 8h). Again, these results suggested that the crystallinity of the minor component of a blend has limited influence on both properties. Moreover, while additional weight loss occurred, the relative blend

https://doi.org/10.1021/acsapm.1c00454
ACS Appl. Polym. Mater. 2021, 3, 3878−3890

composition remained consistent, allowing for mechanical properties to remain stable. However, in the 50 PLA/50 PCL blend system, there is no minor fraction, so either component undergoing hydrolysis would impact the fiber mechanics. In fact, the 50 PLA/50 PCL system exhibits an increase in the strain-at-yield when erosion of both crystalline phases was measured (Figure 8h), and the blend composition shifted from 50 PLA/50 PCL to 35 PLA/65 PCL. Similarly, the same mechanical changes are observed in the 25 PLA/75 PCL system. Interestingly, the only measured structural change was the disappearance of the (110)/(200) crystal reflection and an increase in the PCL mean crystallite size (Figure 8h). While it was previously proposed that the size or amount of minor component crystallinity had little influence on overall mechanics, the disappearance of the PLA-specific reflection yielded a more elastic fiber system. This influence on mechanics by might suggest that the crystallinity of the minor component is able to play a role in bulk mechanics when a drastic change occurs, such as a loss in the dominant reflection.

By week three, the only testable control (control PCL nonwoven fibers) exhibited no significant mechanical changes even though the PCL crystallite size was further reduced (Figure 9a–d). Surprisingly, the 75 PLA/25 PCL system did not follow the control PLA trend of catastrophic mechanical failure due to structural changes. The longevity of the 75 PLA/25 PCL mechanics was quite intriguing given that the nonwoven fibers had suffered a 60% weight loss by week three; we attributed this stability to the consistent blend composition. The 75 PLA/25 PCL system was measured to have a modulus increase that was attributed to the re-emergence of the crystallites associated with the (110)/(200) reflection (Figure 9d). Similarly, the reflection also re-emerged in both the 50 PLA/50 PCL and 25 PLA/75 PCL nonwoven systems (Figure 9d), and an increase in yield stress was measured (Figure 9c). However, the high strain-at-yield values that were measured the previous week in both systems were dramatically reduced (Figure 9b). This loss in elasticity was also attributed to the recrystallization of PLA (Figure 9d).

At the final time point, control PCL nonwoven fibers were measured to have an increase in crystallite size (Figure 9h), as well as a slight weight loss. The combination of large crystallites and large-scale hydrolysis in the control PCL system affected each measured mechanical property. While an increase in the modulus (Figure 9e) and strain-at-yield (Figure 9f) were measured, a decrease in the yield stress was also observed (Figure 9g). It is likely that the larger crystallites improved the modulus, but large-scale chain scission events forced the control PCL nonwoven fibers to be more elastic (Figure 9h). Again, the 75 PLA/25 PCL fibers were tested and were found to have a higher modulus (Figure 9e) and yield stress (Figure 9g) than the previous week. This strength increase was likely due to the increase in the melting enthalpy of the PLA component (Figure 9h). A modulus increase was also observed in the other PLA/PCL blended nonwoven fibers. In the 50 PLA/50 PCL system, an increase in PCL heat of fusion was speculated as the source for the increase in the modulus (Figure 9h). However, the cause of the increase in the modulus (Figure 9e) within the 25 PLA/75 PCL system was not due to an increase in the melting enthalpy. Instead, it was likely the result of the blend composition shift from 10 PLA/90 PCL to 25 PLA/75PCL, which was indicated by ^{1}H NMR (Figure 4b).

CONCLUSIONS

In bioresorbable fiber scaffolds, it is essential to utilize a material with an appropriate degradation profile and that the material maintains mechanical integrity throughout its lifetime. In this work, we demonstrated that the blend composition of coextruded nanofibers greatly impacted the fiber degradation kinetics and mechanical properties over the course of degradation. Furthermore, the properties found in the degradation study are closely coupled to the morphology of the blended nanofibers. For instance, the blended material that demonstrated the most consistent mechanical properties was 75 PLA/25 PCL, which also had the smallest PLA and PCL crystallites. The small crystallite size enhanced the mobility in the amorphous region, leading to the expected degradation profile of the amorphous fraction. By contrast, larger crystallite sizes led to restricted mobility in the amorphous region, leading to early degradation of the crystalline fraction, thus decreasing the mechanical properties over the course of the study. Understanding the hydrolytic effects on coextruded, rectangular fibers further extends the technological impact of multilayer coextrusion in the biomedical field because processing directly impacts morphology and consequently mechanical properties and degradation kinetics.

ASSOCIATED CONTENT

Supporting Information

The Supporting Information is available free of charge at https://pubs.acs.org/doi/10.1021/acsapm.1c00454.

Quantification of fiber isolation via ^{1}H NMR, PLA/PCL fiber dimension determination of blend composition throughout the *in vitro* degradation study, DSC, WAXS, and tensile testing (PDF)

AUTHOR INFORMATION

Corresponding Authors

LaShanda T. J. Korley − *Department of Materials Science and Engineering and Department of Chemical and Biomolecular Engineering, University of Delaware, Newark, Delaware 19716, United States;* orcid.org/0000-0002-8266-5000; Phone: (302) 831-0937; Email: lkorley@udel.edu

Jonathan K. Pokorski − *Department of Nanoengineering and Institute for Materials Discovery and Design, University of California San Diego, La Jolla, California 92093, United States;* orcid.org/0000-0001-5869-6942; Phone: (858) 246-3183; Email: jpokorski@ucsd.edu

Author

Kristian M. Van de Voorde − *Department of Materials Science and Engineering, University of Delaware, Newark, Delaware 19716, United States;* orcid.org/0000-0003-3398-2664

Complete contact information is available at: https://pubs.acs.org/10.1021/acsapm.1c00454

Notes

The authors declare no competing financial interest.

ACKNOWLEDGMENTS

This material is based upon work supported by the National Science Foundation Graduate Research Fellowship Program under grant no. 1247394 and the PIRE: Bio-inspired Materials and Systems (NSF-OISE 1844463). Any opinions, findings,

conclusions, or recommendations expressed in this work are those of the author(s) and do not necessarily reflect the views of the National Science Foundation. Additionally, the characterization suites at the University of Delaware, the Advanced Materials Characterization Laboratory (AMCL) and the Keck Microscopy Center are both acknowledged for access to thermal and spectroscopy characterization instruments. For the use of the multilayer coextrusion facilities at Case Western Reserve University in the NSF STC Center for Layered Polymeric Systems (CLiPS, DMR-0423914), the authors appreciated assistance in composite tape fabrication.

REFERENCES

(1) Sill, T. J.; von Recum, H. A. Electrospinning: Applications in Drug Delivery and Tissue Engineering. *Biomaterials* **2008**, *29*, 1989−2006.
(2) Schiffman, J. D.; Schauer, C. L. A Review: Electrospinning of Biopolymer Nanofibers and their Applications. *Polym. Rev.* **2008**, *48*, 317−352.
(3) Mao, A. S.; Mooney, D. J. Regenerative Medicine: Current Therapies and Future Directions. *Proc. Natl. Acad. Sci. U.S.A.* **2015**, *112*, 14452−14459.
(4) Wang, X.; Ding, B.; Li, B. Biomimetic Electrospun Nanofibrous Structures for Tissue Engineering. *Mater. Today* **2013**, *16*, 229−241.
(5) Vasita, R.; Katti, D. S. Nanofibers and Their Applications in Tissue Engineering. *Int. J. Nanomed.* **2006**, *1*, 15−30.
(6) Kim, S.-E.; Wang, J.; Jordan, A. M.; Korley, L. T. J.; Baer, E.; Pokorski, J. K. Surface Modification of Melt Extruded Poly(ε-caprolactone) Nanofibers: Toward a New Scalable Biomaterial Scaffold. *ACS Macro Lett.* **2014**, *3*, 585−589.
(7) Nair, L. S.; Laurencin, C. T. Biodegradable Polymers as Biomaterials. *Prog. Polym. Sci.* **2007**, *32*, 762−798.
(8) Means, A. K.; Grunlan, M. A. Modern Strategies to Achieve Tissue-Mimetic, Mechanically Robust Hydrogels. *ACS Macro Lett.* **2019**, *8*, 705−713.
(9) Gil-Castell, O.; Badia, J. D.; Bou, J.; Ribes-Greus, A. Performance of Polyester-Based Electrospun Scaffolds under *in Vitro* Hydrolytic Conditions: From Short-Term to Long-Term Applications. *Nanomaterials* **2019**, *9*, 786.
(10) Slomkowski, S. Biodegradable Polyesters for Tissue Engineering. *Macromol. Symp.* **2007**, *253*, 47−58.
(11) O'Brien, F. J. Biomaterials & Scaffolds for Tissue Engineering. *Mater. Today* **2011**, *14*, 88−95.
(12) Sajkiewicz, P.; Heljak, M. K.; Gradys, A.; Choińska, E.; Rumiński, S.; Jaroszewicz, T.; Bissenik, I.; Święszkowski, W. Degradation and Related Changes in Supermolecular Structure of Poly(Caprolactone) in Vivo Conditions. *Polym. Degrad. Stab.* **2018**, *157*, 70−79.
(13) Li, S. Hydrolytic Degradation Characteristics of Aliphatic Polyesters Derived from Lactic and Glycolic Acids. *J. Biomed. Mater. Res.* **1999**, *48*, 342−353.
(14) Woodard, L. N.; Grunlan, M. A. Hydrolytic Degradation and Erosion of Polyester Biomaterials. *ACS Macro Lett.* **2018**, *7*, 976−982.
(15) Pfau, M. R.; McKinzey, K. G.; Roth, A. A.; Grunlan, M. A. PCL-Based Shape Memory Polymer Semi-IPNs: The Role of Miscibility in Tuning the Degradation Rate. *Biomacromolecules* **2020**, *21*, 2493−2501.
(16) Brannigan, R. P.; Heise, A. Synthesis of Mechanically Robust Renewable Poly(Ester-Amide)s through Co-Polymerisation of Unsaturated Polyesters and Synthetic Polypeptides. *Eur. Polym. J.* **2020**, *123*, 109417.
(17) Gaona, L. A.; Gómez Ribelles, J. L.; Perilla, J. E.; Lebourg, M. Hydrolytic Degradation of PLLA/PCL Microporous Membranes Prepared by Freeze Extraction. *Polym. Degrad. Stab.* **2012**, *97*, 1621−1632.
(18) Woodruff, M. A.; Hutmacher, D. W. The return of a forgotten polymer-Polycaprolactone in the 21st century. *Prog. Polym. Sci.* **2010**, *35*, 1217−1256.
(19) Farah, S.; Anderson, D. G.; Langer, R. Physical and mechanical properties of PLA, and their functions in widespread applications - A comprehensive review. *Adv. Drug Deliv. Rev.* **2016**, *107*, 367−392.
(20) Garlotta, D. Literature Review of Poly (Lactic Acid). *J. Polym. Environ.* **2001**, *9*, 63−84.
(21) Bai, H.; Xiu, H.; Gao, J.; Deng, H.; Zhang, Q.; Yang, M.; Fu, Q. Tailoring Impact Toughness of Poly(l-lactide)/Poly(ε-caprolactone) (PLLA/PCL) Blends by Controlling Crystallization of PLLA Matrix. *ACS Appl. Mater. Interfaces* **2012**, *4*, 897−905.
(22) Sikorska, W.; Musioł, M.; Rydz, J.; Zięba, M.; Rychter, P.; Lewicka, K.; Šiškova, A.; Mosnáčková, K.; Kowalczuk, M.; Adamus, G. Prediction studies of environment-friendly biodegradable polymeric packaging based on PLA. Influence of specimens' thickness on the hydrolytic degradation profile. *Waste Manag.* **2018**, *78*, 938−947.
(23) Vieira, A. C.; Vieira, J. C.; Ferra, J. M.; Magalhães, F. D.; Guedes, R. M.; Marques, A. T. Mechanical Study of PLA-PCL Fibers during in Vitro Degradation. *J. Mech. Behav. Biomed. Mater.* **2011**, *4*, 451−460.
(24) Wu, D.; Lin, D.; Zhang, J.; Zhou, W.; Zhang, M.; Zhang, Y.; Wang, D.; Lin, B. Selective Localization of Nanofillers: Effect on Morphology and Crystallization of PLA/PCL Blends. *Macromol. Chem. Phys.* **2011**, *212*, 613−626.
(25) Liu, L.; Li, S.; Garreau, H.; Vert, M. Selective Enzymatic Degradations of Poly(l-lactide) and Poly(ε-caprolactone) Blend Films. *Biomacromolecules* **2000**, *1*, 350−359.
(26) Roy, X.; Sarazin, P.; Favis, B. D. Ultraporous Nanosheath Materials by Layer-by-Layer Deposition onto Co-Continuous Polymer-Blend Templates. *Adv. Mater.* **2006**, *18*, 1015−1019.
(27) Barral, V.; Dropsit, S.; Cayla, A.; Campagne, C.; Devaux, É. Study of the Influence of Pcl on the in Vitro Degradation of Extruded Pla Monofilaments and Melt-Spun Filaments. *Polymers* **2021**, *13*, 171.
(28) Bi, H.; Liu, F.; Wang, M.; Mao, Z.; Zhai, Y.; Li, W.; Wang, S.; Zhang, M. Construction of ultra-stable perovskite-polymer fibre membranes by electrospinning technology and its application to light-emitting diodes. *Polym. Int.* **2021**, *70*, 90−95.
(29) Van de Voorde, K. M.; Pokorski, J. K.; Korley, L. T. J. Exploring Morphological Effects on the Mechanics of Blended Poly(lactic acid)/Poly(ε-caprolactone) Extruded Fibers Fabricated Using Multilayer Coextrusion. *Macromolecules* **2020**, *53*, 5047−5055.
(30) Jordan, A. M.; Korley, L. T. J. Toward a Tunable Fibrous Scaffold: Structural Development during Uniaxial Drawing of Coextruded Poly(ε-caprolactone) Fibers. *Macromolecules* **2015**, *48*, 2614−2627.
(31) Jordan, A. M.; Marotta, T.; Korley, L. T. J. Reducing Environmental Impact: Solvent and PEO Reclamation During Production of Melt-Extruded PCL Nanofibers. *ACS Sustainable Chem. Eng.* **2015**, *3*, 2994−3003.
(32) Lee, J.; Kim, J.; Bae, M.; Park, S.; Balikov, D.; Sung, H.-j.; Jeon, H.; Park, H.; Um, S.; Lee, K.; Kwon, I. Development of Poly(ε-caprolactone) Scaffold Loaded with Simvastatin and Beta-Cyclodextrin Modified Hydroxyapatite Inclusion Complex for Bone Tissue Engineering. *Polymers* **2016**, *8*, 49.
(33) Kim, S.-E.; Harker, E. C.; De Leon, A. C.; Advincula, R. C.; Pokorski, J. K. Coextruded, Aligned, and Gradient-Modified Poly(ε-caprolactone) Fibers as Platforms for Neural Growth. *Biomacromolecules* **2015**, *16*, 860−867.
(34) Fenni, S. E.; Wang, J.; Haddaoui, N.; Favis, B. D.; Müller, A. J.; Cavallo, D. Crystallization and self-nucleation of PLA, PBS and PCL in their immiscible binary and ternary blends. *Thermochim. Acta* **2019**, *677*, 117−130.
(35) Jordan, A. M.; Viswanath, V.; Kim, S.-E.; Pokorski, J. K.; Korley, L. T. J.; Jordan, A. M.; Jordan, A. M.; Kim, S. Processing and surface modification of polymer nanofibers for biological scaffolds: a review. *J. Mater. Chem. B* **2016**, *4*, 5958−5974.
(36) Patterson, A. L. The Scherrer Formula for X-Ray Particle Size Determination. *Phys. Rev.* **1939**, *56*, 978−982.
(37) Li, S. M.; Garreau, H.; Vert, M. Structure-property relationships in the case of the degradation of massive poly(?-hydroxy acids) in aqueous media. *J. Mater. Sci.: Mater. Med.* **1990**, *1*, 131−139.

https://doi.org/10.1021/acsapm.1c00454
ACS Appl. Polym. Mater. 2021, 3, 3878−3890

(38) Shamsah, A. H.; Cartmell, S. H.; Richardson, S. M.; Bosworth, L. A. Material Characterization of PCL:PLLA Electrospun Fibers Following Six Months Degradation in Vitro. *Polymers* **2020**, *12*, 700.
(39) Tsuji, H.; Ikada, Y. Blends of aliphatic polyesters. II. Hydrolysis of solution-cast blends from poly(L-lactide) and poly(?-caprolactone) in phosphate-buffered solution. *J. Appl. Polym. Sci.* **1998**, *67*, 405−415.
(40) Huang, Y.; Chen, F.; Pan, Y.; Chen, C.; Jiang, L.; Dan, Y. Effect of Hydrophobic Fluoropolymer and Crystallinity on the Hydrolytic Degradation of Poly(Lactic Acid). *Eur. Polym. J.* **2017**, *97*, 308−318.
(41) Zhang, C.; Lan, Q.; Zhai, T.; Nie, S.; Luo, J.; Yan, W. Melt Crystallization Behavior and Crystalline Morphology of Polylactide/Poly(ε-caprolactone) Blends Compatibilized by Lactide-Caprolactone Copolymer. *Polymers* **2018**, *10*, 1181.
(42) Tsuji, H.; Mizuno, A.; Ikada, Y. Properties and morphology of poly(L-lactide). III. Effects of initial crystallinity on long-termin vitro hydrolysis of high molecular weight poly(L-lactide) film in phosphate-buffered solution. *J. Appl. Polym. Sci.* **2000**, *77*, 1452−1464.
(43) Kalita, N. K.; Bhasney, S. M.; Mudenur, C.; Kalamdhad, A.; Katiyar, V. End-of-Life Evaluation and Biodegradation of Poly(Lactic Acid) (PLA)/Polycaprolactone (PCL)/Microcrystalline Cellulose (MCC) Polyblends under Composting Conditions. *Chemosphere* **2020**, *247*, 125875.
(44) Di Lorenzo, M. L.; Righetti, M. C.; Cocca, M.; Wunderlich, B. Coupling between Crystal Melting and Rigid Amorphous Fraction Mobilization in Poly(Ethylene Terephthalate). *Macromolecules* **2010**, *43*, 7689−7694.
(45) Wokadala, O. C.; Ray, S. S.; Bandyopadhyay, J.; Wesley-Smith, J.; Emmambux, N. M. Morphology, Thermal Properties and Crystallization Kinetics of Ternary Blends of the Polylactide and Starch Biopolymers and Nanoclay: The Role of Nanoclay Hydrophobicity. *Polymers* **2015**, *71*, 82−92.
(46) Yeo, J. C. C.; Muiruri, J. K.; Tan, B. H.; Thitsartarn, W.; Kong, J.; Zhang, X.; Li, Z.; He, C. Biodegradable PHB-Rubber Copolymer Toughened PLA Green Composites with Ultrahigh Extensibility. *ACS Sustainable Chem. Eng.* **2018**, *6*, 15517−15527.
(47) Gorrasi, G.; Pantani, R. Effect of PLA Grades and Morphologies on Hydrolytic Degradation at Composting Temperature: Assessment of Structural Modification and Kinetic Parameters. *Polym. Degrad. Stab.* **2013**, *98*, 1006−1014.
(48) Bonartsev, A. P.; Boskhomodgiev, A. P.; Iordanskii, A. L.; Bonartseva, G. A.; Rebrov, A. V.; Makhina, T. K.; Myshkina, V. L.; Yakovlev, S. A.; Filatova, E. A.; Ivanov, E. A.; Bagrov, D. V.; Zaikov, G. E. Hydrolytic Degradation of Poly(3-Hydroxybutyrate), Polylactide and Their Derivatives: Kinetics, Crystallinity, and Surface Morphology. *Mol. Cryst. Liq. Cryst.* **2012**, *556*, 288−300.
(49) Sekosan, G.; Vasanthan, N. Morphological changes of annealed poly-ε-caprolactone by enzymatic degradation with lipase. *J. Polym. Sci., Part B: Polym. Phys.* **2010**, *48*, 202−211.
(50) Allen, N. S.; Edge, M.; Mohammadian, M.; Jones, K. Hydrolytic Degradation of Poly(Ethylene Terephthalate): Importance of Chain Scission versus Crystallinity. *Eur. Polym. J.* **1991**, *27*, 1373−1378.
(51) Dhanvijay, P. U.; Shertukde, V. V. Review: Crystallization of Biodegradable Polymers. *Polym.-Plast. Technol. Eng.* **2011**, *50*, 1289−1304.
(52) Jariyasakoolroj, P.; Rojanaton, N.; Jarupan, L. Crystallization Behavior of Plasticized Poly(Lactide) Film by Poly(l-Lactic Acid)-Poly(Ethylene Glycol)-Poly(l-Lactic Acid) Triblock Copolymer. *Polym. Bull.* **2020**, *77*, 2309−2323.
(53) Broz, M.; Vanderhart, D. L.; Washburn, N. R. Structure and mechanical properties of poly(?,?-lactic acid)/poly(ε-caprolactone) blends. *Biomaterials* **2003**, *24*, 4181−4190.
(54) Bessell, T. J.; Hull, D.; Shortall, J. B. The Effect of Polymerization Conditions and Crystallinity on the Mechanical Properties and Fracture of Spherulitic Nylon 6. *J. Mater. Sci.* **1975**, *10*, 1127−1136.

https://doi.org/10.1021/acsapm.1c00454
ACS Appl. Polym. Mater. 2021, 3, 3878−3890